Simulation of vector fields with arbitrary second-order correlations

Brynmor J. Davis

*The Beckman Institute for Advanced Science and Technology
and the Department of Electrical and Computer Engineering,
University of Illinois at Urbana-Champaign, 405 North Mathews Avenue, Urbana, IL 61820*

bryn@uiuc.edu

Abstract: Temporally-stationary electromagnetic fields with arbitrary second-order coherence functions are simulated using standard statistical tools. In cases where the coherence function takes a commonly-used separable form, a computationally-efficient variation of the approach can be applied. This work provides a generalization of previous spatio-temporal simulators which model only scalar fields and require either restrictions on the coherence function or consider only two points in space. The simulation of a partially-polarized Gaussian Schell-model beam and a partially-radially-polarized beam are demonstrated.

© 2007 Optical Society of America

References and links

1. L. Mandel and E. Wolf, *Optical Coherence and Quantum Optics* (Cambridge University Press, 1995).
2. J. W. Goodman, *Statistical Optics* (Wiley-Interscience, 1985).
3. G. Gbur, "Simulating fields of arbitrary spatial and temporal coherence," Opt. Express **14**, 7567–7578 (2006), http://www.opticsinfobase.org/abstract.cfm?URI=oe-14-17-7567 .
4. E. Wolf, "Correlation-induced changes in the degree of polarization, the degree of coherence, and the spectrum of random electromagnetic beams on propagation," Opt. Lett. **28**, 1078–1080 (2003).
5. P. Vahimaa and J. Turunen, "Finite-elementary-source model for partially coherent radiation," Opt. Express **14**, 1376–1381 (2006), http://www.opticsinfobase.org/abstract.cfm?URI=oe-14-4-1376 .
6. A. M. Zysk, P. S. Carney, and J. C. Schotland, "Eikonal method for calculation of coherence functions," Phys. Rev. Lett. **95** (043904) (2005).
7. E. Wolf, "Invariance of the spectrum of light on propagation," Phys. Rev. Lett. **56**, 1370–1372 (1986).
8. G. Magyar and L. Mandel, "Interference fringes produced by superposition of two independent Maser light beams," Nature **198**, 255–256 (1963).
9. B. Davis, E. Kim, and J. R. Piepmeier, "Stochastic modeling and generation of partially polarized or partially coherent electromagnetic waves," RadioSci. **39** (RS1001) (2004).
10. R. Simon and N. Makunda, "Twisted Gaussian Schell-model beams," J. Opt. Soc. Am. A **10**, 95–109 (1993).
11. E. Wolf and G. S. Agarwal, "Coherence theory of laser resonator modes," J. Opt. Soc. Am. A **1**, 541–546 (1984).
12. Y. Cai and S. He, "Propagation of a partially coherent twisted anisotropic Gaussian Schell-model beam in a turbulent atmosphere," Appl. Phys. Lett. **89** (041117) (2006).
13. E. Tervonen, J. Turunen, and A. T. Friberg, "Transverse Laser-mode structure determination from spatial coherence measurements: experimental results," Appl. Phys. B **49**, 409–414 (1989).
14. L. D. A. Lundeberg, G. P. Lousberg, D. L. Boiko, and E. Kapon, "Spatial coherence measurements in arrays of coupled vertical cavity surface emitting lasers," Appl. Phys. Lett. **90** (121103) (2007).
15. D. F. V. James, "Change of polarization of light beams on propagation in free space," J. Opt. Soc. Am. A **11**, 1641–1643 (1994).
16. O. Korotkova, M. Salem, and E. Wolf, "The far-zone behavior of the degree of polarization of electromagnetic beams propagating through atmospheric turbulence," Opt. Commun. **233**, 225–230 (2004).
17. G. H. Golub and C. F. Van Loan, *Matrix Computations* (Johns Hopkins University Press, 1996).

---

18. J. H. Michels, P. K. Varshney, and D. D. Weiner, "Synthesis of correlated multichannel random processes," IEEE Trans. Signal Process. **42**, 367–375 (1994).
19. A. Papoulis and S. U. Pillai, *Probability, Random Variables and Stochastic Processes* (McGraw-Hill, 2002).
20. W. H. Carter and E. Wolf, "Coherence and radiometry with quasihomogeneous planar sources," J. Opt. Soc. Am. **67**, 785–796 (1977).
21. R. Loudon, *The Quantum Theory of Light* (Oxford University Press, 2000).
22. F. Gori, M. Santarsiero, G. Piquero, R. Borghi, A. Mondello, and R. Simon, "Partially polarized Gaussian Schell-model beams," J. Opt. A **3**, 1–9 (2001).
23. N. Hodgson and H. Weber, *Laser Resonators and Beam Propagation: Fundamentals, Advanced Concepts and Applications* (Springer, 2005).
24. K. C. Toussaint, Jr., S. Park, J. E. Jureller, and N. F. Scherer, "Generation of optical vector beams with a diffractive optical element interferometer," Opt. Lett. **30**, 2846–2848 (2005).
25. S. Quabis, R. Dorn, and G. Leuchs, "Generation of a radially polarized doughnut mode of high quality," Appl. Phys. B **81**, 597–600 (2005).
26. P. M. Lurie and M. S. Goldberg, "An approximate method for sampling correlated random variables from partially-specified distributions," Manage. Sci. **44**, 203–218 (1998).

1. Introduction

The non-deterministic nature of light is well known and is the subject of a significant body of literature, e.g. [1, 2]. Stochastic electromagnetic behavior may be taken to arise from fluctuations in the primary source of the field and/or from the interaction of the field with some random medium. While a time- and space-dependent probability density function (PDF) is required to completely define a non-deterministic classical electromagnetic field, physical measurements do not capture this full description. Optical detectors typically measure a time integral of the square magnitude of the impinging field. As a result, the second-order moments of the PDF are directly related to physical measurements and are foremost among the parameters used in the characterization of stochastic electromagnetic fields. The average intensity, spatial and temporal coherence lengths and the polarization state are all determined by the second-order coherence function. This work describes the numerical generation of a discrete random process that can be used to simulate a temporally-stationary electromagnetic field with arbitrary second-order correlation properties.

The simulation of a stochastic scalar field was recently demonstrated [3]. This computational method generates a random process as a function of two spatial coordinates and time. The random process represents a scalar field and can be used in a wide range of numerical experiments. Visualization of the instantaneous intensity of a partially-coherent Gaussian Schell-model beam [1] was demonstrated, as was the effect of its propagation through a random medium.

The effect of propagation on coherence functions is dictated by analytic relations [1, 4] but these can be difficult to evaluate in many cases of interest. Numerical approaches (e.g. [5]) can be applied or simplifications such as geometrical propagation can be used in some circumstances [6]. A beam simulator provides a complementary tool as it allows the random field to be generated, propagated numerically and the coherence function estimated from the output. More generally, the simulated beam can be used as an input to any field-based numerical model of an optical system and the output used in Monte Carlo investigations of the (possibly stochastic) optical system or the properties of the resultant field. By simulating the random process, rather than computing the correlation functions, it is possible to gain insight into the short-time behavior of the quantities of interest, rather than just their effects in the long-time measurements. Additionally, one can envision the numerical demonstration of analytical or experimental results from coherence theory, such as propagation-induced spectral shifts [7] or the observation of interference effects from uncorrelated sources using short-time-average measurements [8].

The simulator detailed in this work generalizes that described in [3] and also of earlier work [9] that considered the simulation of a scalar field at two points, or a vector field at a single

point. Specifically, the simulator described here has no restrictions on the coherence function that can be modeled and a vector field is generated. The form of the coherence function required in [3] excludes the simulation of certain fields, e.g. Twisted Anisotropic Gaussian Schell-Model (TAGSM) beams [10] or the partially-coherent output from a laser or waveguide with more than one non-zero mode [11]. Restrictions on the form of the coherence function also appear in related literature [5]. The model presented here has no such restrictions and can therefore be used to numerically investigate phenomena such as the propagation of TAGSM beams [12] or the estimation of mode distribution from the spatial coherence of a laser [13]. The coherence of fields produced by arrays of correlated sources is also of practical interest (e.g. [14]) and their numerical simulation would not be possible with previous partially-coherent-field simulators. The vector nature of the new model also represents a significant generalization as effects such as propagation-induced polarization change [15] or the influence of random media on the polarization state [16] are now encompassed.

2. Generating the Field

The second-order statistics of a stationary two-dimensional electric field are described by the coherence function,

$$\Gamma_{jj'}(x,y,x',y',\tau) = <\mathscr{E}_j(x,y,t)\mathscr{E}_{j'}^*(x',y',t-\tau)>, \tag{1}$$

where j and j' can take on the values x or y, and $\mathscr{E}_j(x,y,t)$ is the electric field at spatial coordinates (x,y), at time t and in direction j. Here a script typeface is used to indicate a random quantity and angle braces indicate an expected value. The electric field is assumed to be stationary so Γ depends on τ but not t. Ergodicity is also assumed so that a temporal average over one realization of the random field is equivalent to an ensemble average, at any given t, over many realizations of the field.

The algorithms developed in this paper generate a random variable with user defined second-order statistics for a discrete set of (j,x,y,t) values. Two different algorithms will be given. The first case is applicable to any coherence function Γ and will be known as the 'general' case. The general case produces a random variable at any user-defined set of spatial (x,y) points and field directions j at these points. This set of (j,x,y) values will be mapped to a one-dimensional vector and the location in this vector indexed by the integer n. The temporal axis is assumed to be regularly sampled at or above the Nyquist rate and with samples indexed by m. Thus the values of the continuous coherence function $\Gamma_{jj'}(x,y,x',y',\tau)$ at the points of interest are used to define a discrete coherence function $\Gamma[n,n',m-m']$. Here curved brackets ( ) are used to indicate continuous variables and square brackets [ ] indicate discrete variables.

The second case is said to be 'separable' and requires the coherence function to be factorable into a particular form. This form arises frequently in coherence theory and is similar to that required in [3], but with a generalization to vector fields. In the separable case the form of the coherence function is exploited to allow a significantly more efficient algorithm. The separable algorithm also requires that the x, y and t directions are regularly sampled at a rate satisfying the Nyquist criterion and that j takes on values of both x and y at all spatio-temporal points (*i.e.* all field directions are considered). The sampled x and y axes are then indexed by k and l respectively. As a result, the values of the continuous coherence function $\Gamma_{jj'}(x,y,x',y',\tau)$ at the sample points are used to define a discrete coherence function $\Gamma_{jj'}[k,l,k',l',m-m']$.

The algorithms described here start with a set of uncorrelated random variables, which are linearly manipulated to produce a set of discrete-time random processes that have the desired second-order correlation properties. The input random variables can be realized in simulation by using random number generators — specific examples of this are given later in the paper. The linear manipulations involve scaling and shift-invariant filtering in the separable case; and

random variable summation using the Cholesky decomposition [17] and shift-invariant filtering in the general case. Both of these techniques are standard methods of manipulating the statistics of random processes [18, 19]. The resulting complex random processes represent the complex amplitude field at the discrete points of interest.

2.1. The General Case

The algorithm starts with one complex random variable for each discrete point considered. These input processes $\mathscr{X}$ have second-order correlations given by,

$$< \mathscr{X}[n,m]\mathscr{X}^*[n',m'] >= \delta[n-n']\delta[m-m'], \tag{2}$$

where $\delta[\cdot]$ is the discrete-argument delta function. These input random variables will be manipulated to give a discrete field $\mathscr{E}$ that exhibits the required second-order correlations.

Consider the discrete-time Fourier transform of the coherence function,

$$W[n,n',\omega] = \sum_u \Gamma[n,n',u]e^{-i\omega u}. \tag{3}$$

This can be regarded as a matrix function of angular frequency $\bar{W}(\omega)$, with n and n' indexing the rows and columns respectively and $^-$ denoting a matrix. Since the matrix is a discrete representation of the cross-spectral density, it is guaranteed to be Hermitian and positive semi-definite [1]. This means that it can be decomposed using the Cholesky decomposition to give a matrix $\bar{V}(\omega)$ such that $\bar{V}(\omega)\bar{V}^\dagger(\omega) = \bar{W}(\omega)$, where † represents the Hermitian (conjugate transpose). Writing this explicitly,

$$W[n,n',\omega] = \sum_r V[n,r,\omega]V^*[n',r,\omega]. \tag{4}$$

It is then useful to define a set of temporal filters,

$$h_V[n,r,m] = \frac{1}{2\pi} \int_{-\pi}^{\pi} V[n,r,\omega]e^{i\omega m}d\omega. \tag{5}$$

The output random variables, which simulate the field, can then be calculated as,

$$\mathscr{E}[n,m] = \sum_r \sum_q h_V[n,r,m-q]\mathscr{X}[r,q]. \tag{6}$$

This equation describes the implementation of the general algorithm.

Eq. (6) is a discrete convolution over the time axis and a summation over all the input processes. Taking the cross correlation, it can be shown that,

$$\begin{aligned}
< \mathscr{E}[n,m]\mathscr{E}^*[n',m'] > &= \frac{1}{2\pi} \int_{-\pi}^{\pi} W[n,n',\omega]e^{i\omega(m-m')}d\omega, \\
&= \Gamma[n,n',m-m'].
\end{aligned} \tag{7}$$

This verifies that the method described by Eq. (6) produces random processes with the desired second-order correlations.

The quantity W is the discrete cross spectral density of the field to be simulated. The Cholesky decomposition is used to find V such that Eq. (4) is satisfied but it would also be possible to use an eigenvector-based approach as given by the Karhunen-Loève decomposition [19]. Such a decomposition would lead to a synthesis of the field according to the principles of the coherent mode representation [1] — $V[n,r,\omega]$ would be the rth coherent mode at frequency

ω. Algorithms for both Cholesky and eigenvector-based matrix decompositions are well studied [17] but the Cholesky decomposition is chosen here as it guarantees $V[n, r, \omega] = 0$ for $r > n$. This means that fewer filters h_V need to be calculated and stored. In both the Cholesky and eigenvector-based methods, significant computational savings can be realized if W is sparse. Efficient algorithms exist for sparse decomposition [17] and fewer non-zero h_V filters will be produced.

2.2. The Separable Case

In the separable case all dimensions are assumed to be regularly sampled on a grid with a sampling rate satisfying the Nyquist criterion. Without loss of generality, the sampling rates will be normalized to 1. The coherence function is assumed to take the separable form,

$$\Gamma_{jj'}[k, l, k', l', m - m'] = A_j[k, l] A_{j'}^*[k', l'] B_{jj'} \eta[k - k', l - l'] R[m - m']. \tag{8}$$

As a reminder, k and l are the discrete spatial indices, while m and j continue to index time and the field direction respectively. In Eq. (8), $A_j[k, l]$ controls the local scale of the coherence function, $B_{jj'}$ determines the relation between the x- and y-polarized fields, $\eta[k - k', l - l']$ determines the spatial coherence and $R[m - m']$ determines the temporal coherence. $B_{jj'}$ obeys the constraints $B_{xx} = B_{yy} = 1$, $B_{yx} = B_{xy}^* = b$ and $|b| \le 1$. Additionally, if the magnitudes of $A_x[k, l]$ and $A_y[k, l]$ are equal, $|b|$ is the degree of polarization [1] at $[k, l]$. The functions η and R are correlation functions and must satisfy the standard positive-semidefiniteness conditions.

The separability of the factor η shown in Eq. (8) implies the degree of spatial coherence is uniform across the x-y plane. While this is a restrictive assumption, it is often seen in the literature and results in what is typically referred to as either a Schell-model or quasihomogeneous [20] source. The separability of R in Eq. (8) implies that the temporal spectrum of the field does not change with space or field direction. In an earlier simulator [3] an assumption analogous to Eq. (8) was used and as mentioned in Sec. 1, this does not allow the simulation of a significant number of practically-important fields.

As with the general case, input random variables are uncorrelated so that,

$$< \mathscr{X}_j[k, l, m] \mathscr{X}_{j'}[k', l', m'] > = \delta_{jj'} \delta[k - k'] \delta[l - l'] \delta[m - m'], \tag{9}$$

where $\delta_{jj'}$ is the Kronecker delta. The constraints on B guarantee that it is a positive semi-definite tensor, so the Cholesky decomposition can be used to define the matrix factor $\bar{H}$ such that,

$$\bar{H} \bar{H}^\dagger = \bar{B} = \begin{bmatrix} B_{xx} & B_{xy} \\ B_{yx} & B_{yy} \end{bmatrix}. \tag{10}$$

Explicitly,

$$\bar{H} = \begin{bmatrix} 1 & 0 \\ b & \sqrt{1 - |b|^2} \end{bmatrix}. \tag{11}$$

Analogous decompositions for η and R can be found such that,

$$R[m] = \sum_q h_R[q] h_R^*[q - m], \tag{12}$$

$$\eta[k, l] = \sum_{o, p} h_\eta[o, p] h_\eta^*[o - k, p - l]. \tag{13}$$

For example, $h_\eta[o, p]$ can be found by Fourier-transforming $\eta[k, l]$ to $\hat{\eta}(\omega_1, \omega_2)$, taking the positive square root ($\hat{\eta}$ is real and non-negative as it is a power spectral density) to get $\hat{h}_\eta(\omega_1, \omega_2)$ and then inverse Fourier transforming to find $h_\eta[o, p]$.

The desired random process can then be constructed as,

$$\mathscr{E}_j[k,l,m] = A_j[k,l] \sum_q h_R[m-q] \sum_o \sum_p h_\eta[k-o,l-p] \sum_{s=x,y} H_{js} \mathscr{X}_s[o,p,q], \qquad (14)$$

where the matrix $\bar{H}$ relates to $H_{jj'}$ in the same way that $\bar{B}$ relates to $B_{jj'}$ in Eq. (10).

From Eq. (14) it is easily verified that $< \mathscr{E}_j[k,l,m]\mathscr{E}_{j'}^*[k',l',m'] >= \Gamma_{jj'}[k,l,k',l',m-m']$. The processing described in Eq. (14) consists of linear shift-invariant filtering to produce the desired spatial and temporal coherence characteristics, a linear combination of the x- and y-polarized input fields to produce the desired polarization relation and multiplication by spatial amplitude profiles. This processing will be much less computationally expensive than that required for the general case. If the field considered has $N \times N$ spatial samples, the general case will require the calculation and implementation of approximately $2N^4$ temporal filters, while the most expensive operation in the separable algorithm can be implemented using $N \times N$ Fast Fourier transforms (or $(N+M-1) \times (N+M-1)$ transforms if h_η is $M \times M$ and discrete-Fourier wrap-around effects are to be avoided).

3. Examples

The generation of two example fields is described in this section. A vectorial Gaussian Schell-model beam is simulated to demonstrate the separable-Γ algorithm and a partially-radially-polarized beam is simulated to demonstrate the general-Γ algorithm. In both cases the input random variables $\mathscr{X}$ are simulated using standard Gaussian random number generators. In addition to satisfying Eq. (2) or Eq. (9), each random variable is zero-mean and complex with a variance of 0.5 in each of the real and imaginary parts and no real-imaginary correlation. The linear processing maintains the Gaussian PDF structure so the generated field $\mathscr{E}$ is also Gaussian. This corresponds to thermal or chaotic light [21] and the PDF of the field is completely determined by Γ.

3.1. The Separable Case: A Gaussian Schell-Model Beam

A vectorial Gaussian Schell-model [22] satisfies the separable form shown in Eq. (8). Such a beam will be simulated here on a 12×12 spatial grid (normalized units) with 5 samples per spatial unit. The temporal axis is 1000 units long with one sample per unit. The constituent functions of Eq. (8) are Gaussian with the following parameters: A has unit amplitude and a second-order moment of 4 for both the x and y field directions; η is unit amplitude and has a second-order moment of 1; R has unit amplitude and a second-order moment of 4; B is defined by $b = 0.5$. The filter h_η is truncated to 20 samples and h_R is truncated to 12 samples. Truncation allows the random field to be generated using a finite number of input random variables.

The random process is generated using Eq. (14) and ergodicity allows the coherence function to be estimated by replacing the expectation operator in Eq. (1) with a discrete average over time. The local coherence properties at a point (x,y) can be decomposed as,

$$\Gamma_{jj'}(x,y,x,y,0) = I(x,y) \left\{ [1-P(x,y)]\frac{\delta_{jj'}}{2} + P(x,y)p_j(x,y)p_{j'}^*(x,y) \right\}, \qquad (15)$$

where $I(x,y)$ is the average intensity, $P(x,y)$ is the degree of polarization and $p_j(x,y)$ represents the normalized complex amplitude of the fully-polarized field component in the j direction [1]. The resulting estimates of these measures along with $|\Gamma_{xx}(x,y,0,0,0)|$ (measures spatial coherence), $|\Gamma_{xx}(0,0,0,0,\tau)|$ (measures temporal coherence) and the instantaneous intensity are shown in Fig. 1. There is strong agreement between the specified values and those calculated from the realized random processes. Note that only the real part of the vector $\mathbf{p}(x,y)$ is used

to plot the field direction, however this is justified as the estimated coherence shows that the intensity of the imaginary component is less than 2% of the intensity of the real component at all spatial points. This agrees with the specification of Γ, which defines a linearly polarized field.

3.2. The General Case: A Partially-Radially-Polarized Beam

To demonstrate the general method given by Eq. (6), the local properties of Eq. (15) will be used to describe a partially-polarized, partially-coherent radially polarized beam [23]. The spatial and temporal coherence will be included by multiplying these local properties with the functions η and R from the Gaussian-Schell example and the degree of polarization will be 0.5.

A fully-radially-polarized beam is known as the TEM_{01}^* mode of a laser when Gauss-Laguerre functions are used to describe the modes. The TEM_{01}^* mode is the sum of a TEM_{01} mode and a TEM_{10} mode with orthogonal polarization directions. This simple mathematical representation is not trivial to reproduce experimentally (e.g. [24, 25]), where the presence of additional modes may result in a reduction of spatial coherence and/or degree of polarization. The example considered here has $P(x,y) = 0.5$, $[p_x(x,y), p_y(x,y)] = [x,y]/\sqrt{x^2+y^2}$ and $I(x,y)$ equal to the intensity of the TEM_{01}^* mode.

The resulting coherence function no longer satisfies Eq. (8), as B would have to be a function of x and y (note that a fully-radially-polarized beam can be cast in the form of Eq. (8) by setting $b = 1$ and having A_x and A_y equal to the appropriate TEM_{01} and TEM_{10} modes). The fully-general method was used to generate the partially-radially-polarized field although it should be noted that a hybrid separable-general method could have been employed. If B is allowed to vary with (x,y) and H is defined according to Eq. (10), then using $H_{js}(x,y)$ in Eq. (14) would allow the generation of a field with the prescribed spatially-varying polarization properties. This hybrid method would set the polarization state at each point with dedicated processing but the separable nature of the spatial and temporal coherence would be exploited to affect computational gains. The fully-general method was used in the example presented here as a proof-of-concept.

The radially-polarized field was realized on the same grid used for the Gaussian-Schell example, although there is now no requirement to use a regularly-spaced spatial grid. The fact that η and R describe coherence functions that drop to zero at a finite range (due to the truncation of the filters in the previous example) makes the Cholesky decomposition much more tractable. It reduces the number of non-zero entries in the correlation matrix $\bar{W}(\omega)$ and therefore eases storage requirements. It also reduces numerical complications in the Cholesky decomposition that might arise due to round-off errors in the tails of the coherence functions.

The results seen in Fig. 2 again show excellent agreement between the expected and observed values. Note that the degree of polarization is undefined at the origin as the intensity is zero. The intensity of the complex component of $\mathbf{p}(x,y)$ is again small — less than 2% of the intensity of the real part at all spatial points.

4. Conclusions and Outlook

A method for simulating spatio-temporal stochastic electromagnetic fields has been presented. The random processes generated can be used in numerical experiments where the non-deterministic behavior of light is important. Unlike previous simulators, there are no restrictions on the coherence properties and vectorial fields are modeled. This allows the simulation of a variety of fields that cannot be simulated with previous methods — for example, partially-polarized beams, multi-mode light from lasers or waveguides, twisted anisotropic Gaussian Schell-model beams and fields produced by arrays of correlated sources.

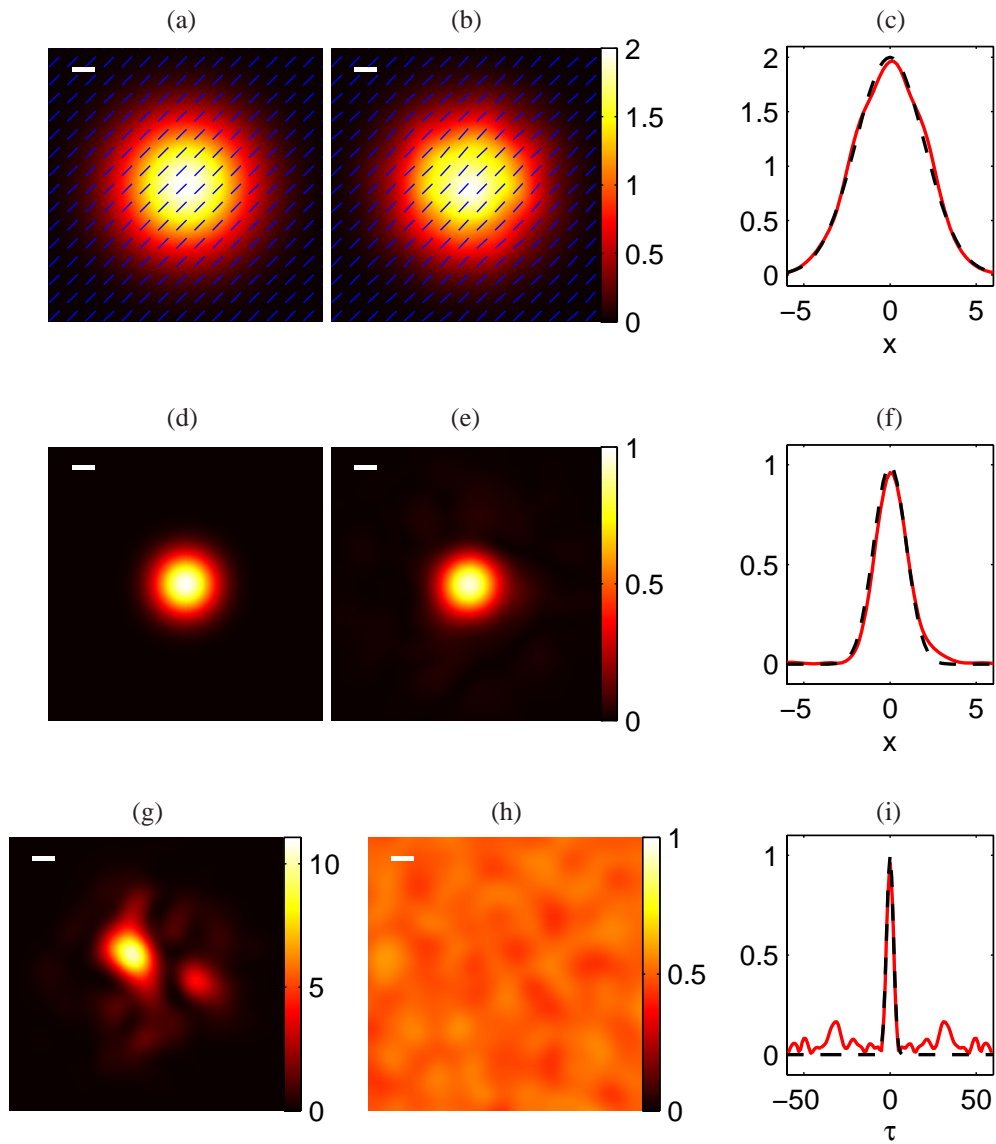One can also envision straight-forward extensions of this work where temporally non-

Fig. 1. Realized and specified coherence properties for the Gaussian-Schell example. The specified intensity $I(x,y)$ and field direction $\mathbf{p}(x,y)$ (in blue) are shown in (a) and the realized values in (b). The white bar indicates one spatial unit. An overlay of x-axis cross sections from (a) and (b) is shown in (c), where the dashed line gives the specified profile. Specified and realized images of $|\Gamma_{xx}(x,y,0,0,0)|$ are shown in (d) and (e) respectively, with an x-axis cross section in (f). A movie (1.4MB) showing 100 consecutive frames of the instantaneous intensity is given in (g). The realized degree of polarization $P(x,y)$ is shown in (h) while the specified value was $P = b = 0.5$. A temporal correlation $|\Gamma_{xx}(0,0,0,0,\tau)|$ is shown in (i).
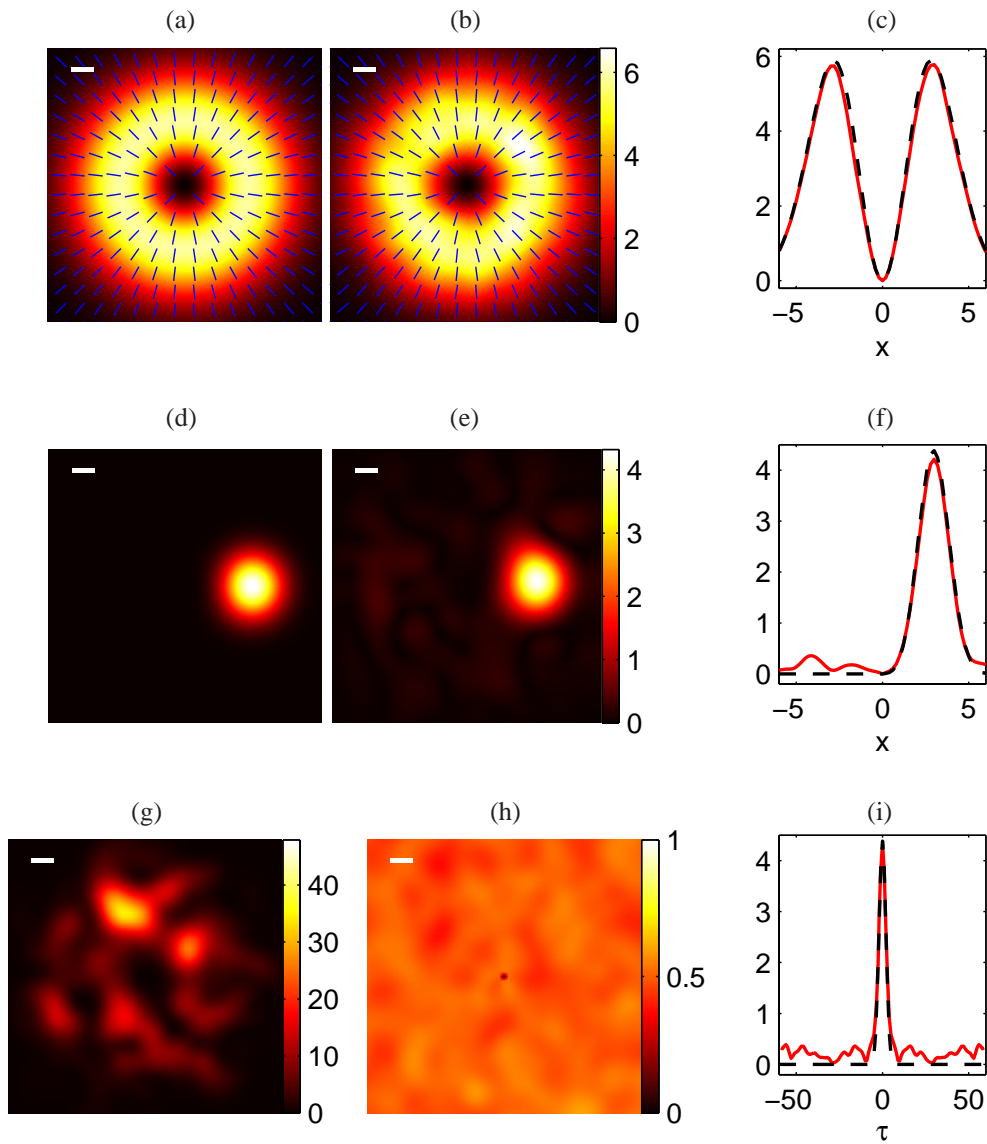
Fig. 2. Realized and specified coherence properties for the radially-polarized example. The specified intensity $I(x,y)$ and field direction $\mathbf{p}(x,y)$ (in blue) are shown in (a) and the realized values in (b). The white bar indicates one spatial unit. An overlay of x-axis cross sections from (a) and (b) is shown in (c), where the dashed line gives the specified profile. Specified and realized images of $|\Gamma_{xx}(x,y,3,0,0)|$ are shown in (d) and (e) respectively, with an x-axis cross section in (f). A movie (1.4MB) showing 100 consecutive frames of the instantaneous intensity is given in (g). The realized degree of polarization $P(x,y)$ is shown in (h) while the specified value was $P = 0.5$. A temporal correlation $|\Gamma_{xx}(0,0,3,0,\tau)|$ is shown in (i).

stationary fields are considered. However this would involve an increase in dimensionality as the absolute time t would need to be included. As a result, substantially more computational effort would be required. In the examples shown here a Gaussian input process produced a Gaussian simulated field. If non-Gaussian distributions are desired the relation between input and output random variables is less clear. However, there is the potential to include non-Gaussian statistics using similar random-process generation methods, e.g. [26]. This would allow the simulation of non-thermal light.

Acknowledgments